Supplemental Information

Supplemental Figures

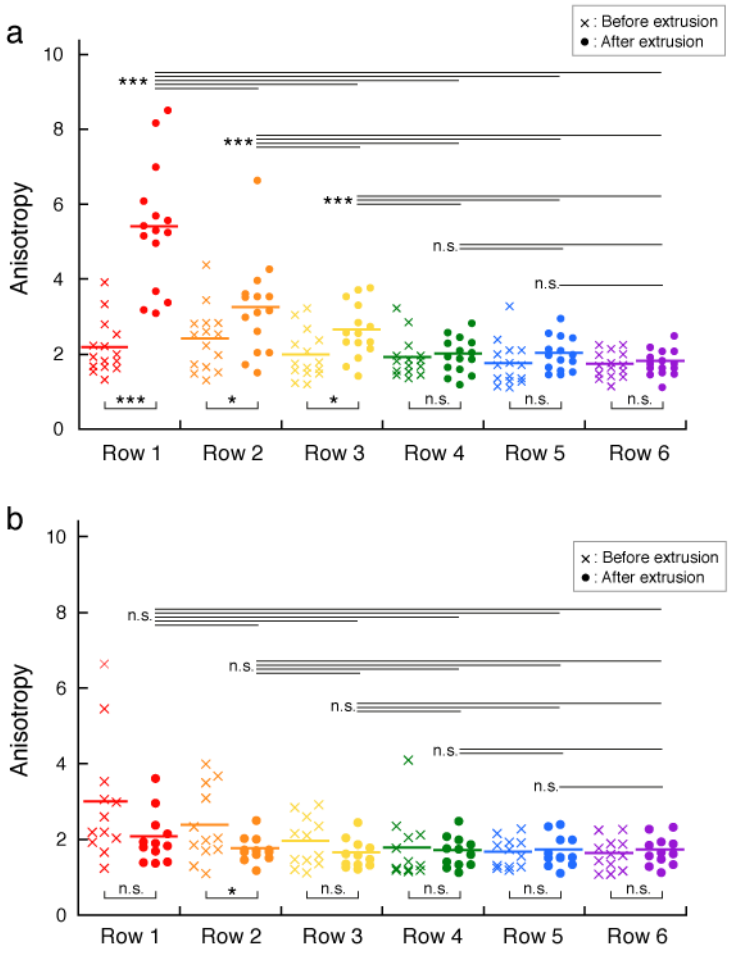

Fig. S1. Quantification of cell shape deformation of histoblasts upon extrusion of boundary LEC. (a and b) Plots of anisotropy of cell shape (Supplemental Materials and Methods) before (crosses) and after (filled circles) the boundary cell extrusions, as a function of distance (i.e., number of rows) from the boundary LECs (n=15 from 3 pupae). Data from wild-type pupae (a) and pupa expressing sqh-RNAi only in LECs (b). *: $p<0.05$, ***: $p<0.001$, n.s.: no significance.

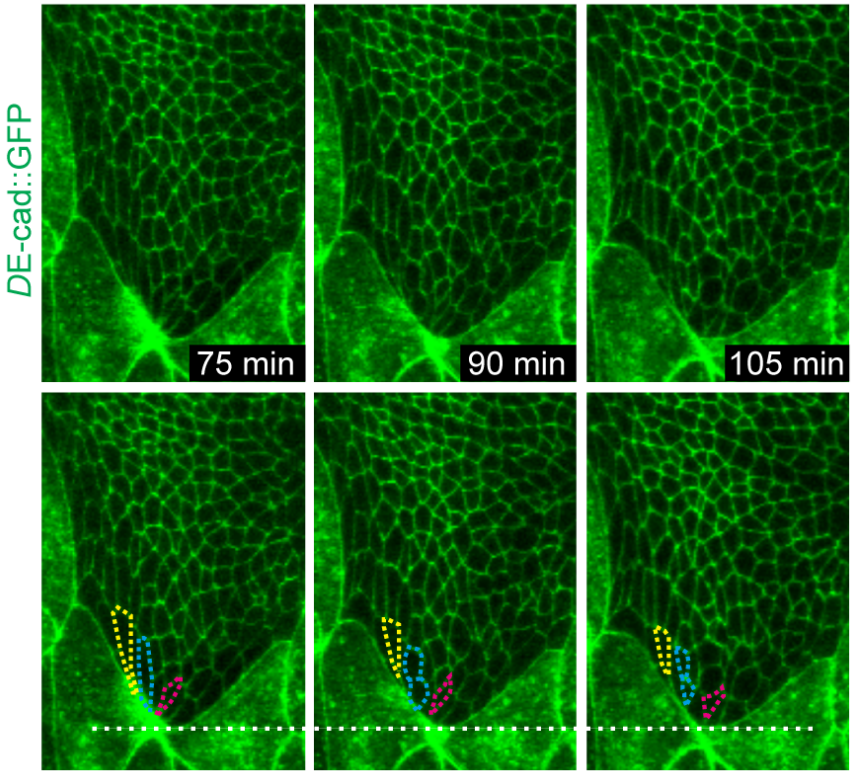

Fig. S2. Fate of the elongated histoblasts after the completion of apical constriction of apoptotic LEC. Confocal fluorescence images of wild type pupa expressing *D*E-cad::GFP, showing the fate of the elongated histoblasts presented in Fig. 1 b and 1c. The first time frame (denoted as 75 min) is the same image as the last frame of Fig. 1b (denoted as 75 min). The elongated histoblasts underwent either cell division (highlighted with blue dotted line) or cell-cell junction remodeling (highlighted with yellow and red dotted lines) after the completion of cell extrusion. White dotted line denotes the edge of the histoblasts.

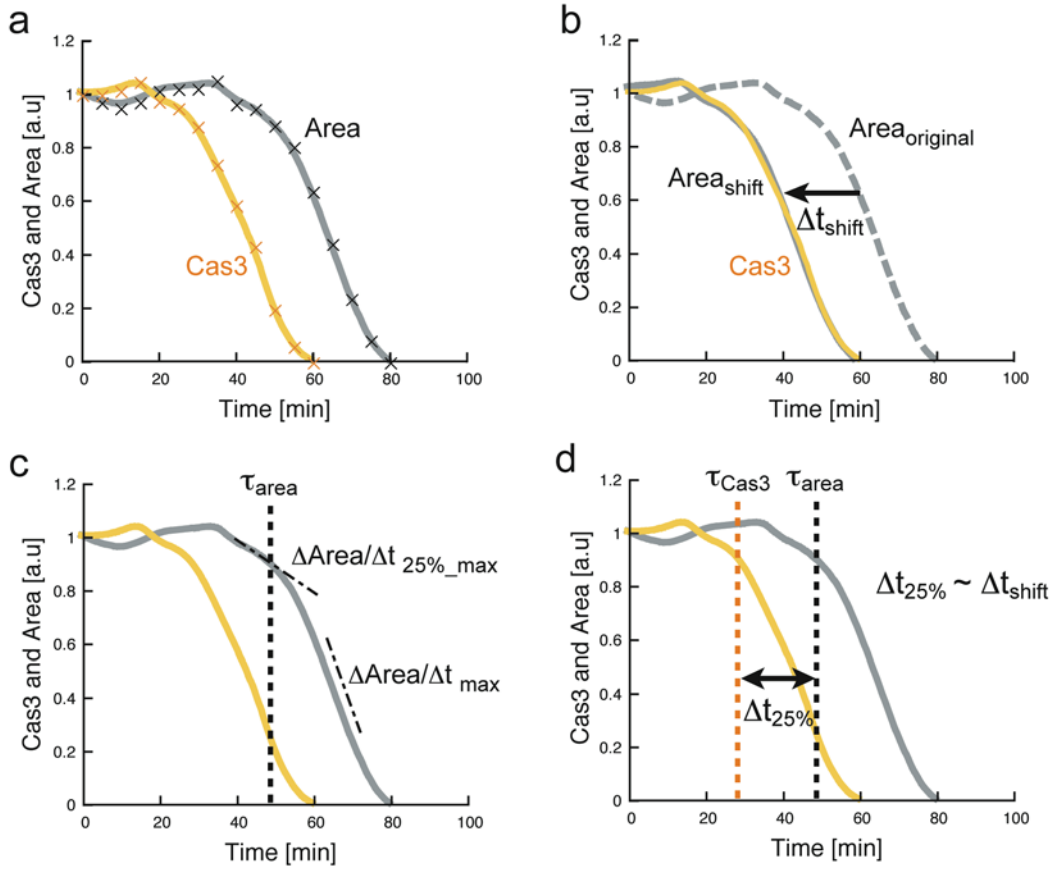

Fig. S3. Determination of transition time. Refer to Materials and methods for more detail. (a) Graphs showing the normalized apical area (gray line) and caspase-3 activity (orange) of apoptotic cell over time. (b) Original Area graph ($Area_{original}$, gray dotted line) was shifted by Δt_{shift} so that the difference between shifted area ($Area_{shift}$, gray solid line) and caspase-3 data (orange line) is minimized. Note gray and orange solid lines are overlapping each other. (c) Transition time of cell area, τ_{area} was determined as the time when the derivative of the graph ($\Delta Area/\Delta t$) reached to 25% of the maximum slope ($\Delta Area/\Delta t_{max}$). (d) The time delay between the initiation of apical constriction and caspase-3 activation measured by 25% of maximum slope, $\Delta t_{25\%} = |\tau_{area} - \tau_{Cas3}|$, was consistent to Δt_{shift}.

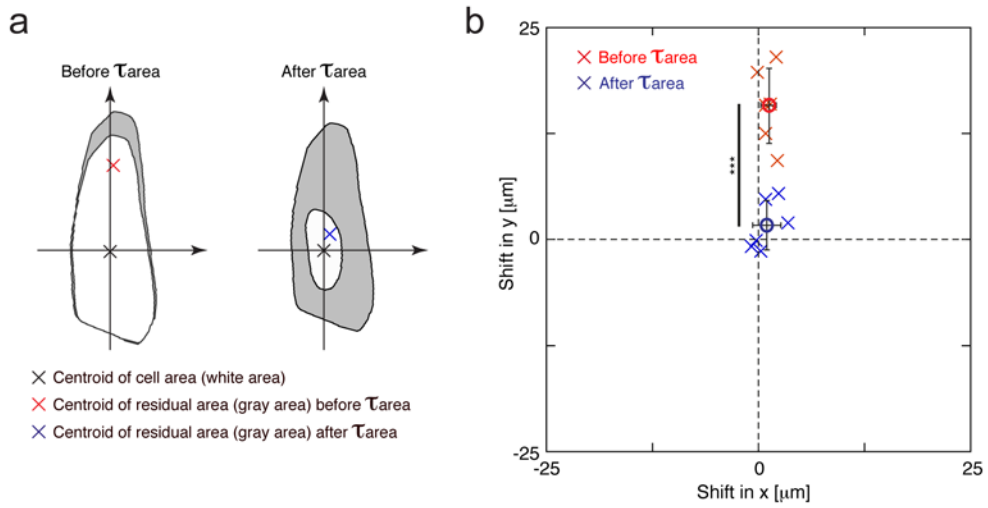

Fig. S4. Quantitative analyses of the deformation in the shape of extruding LECs. (a) Two contour plots showing the cell shape of different time points (25 min apart) for before (left) and after (right) τ_{area}. Black cross denotes the centroid of the cell area at later time point (white in the figure). Red and blue crosses denote the centroid of residual area (difrence between two contour plots, gray in the figure) at before and after τ_{area}, respectively. (b) Summary of 6 data. Open circles and error bars represent the average values and the STDEV, respectively. ***: $p<0.001$.

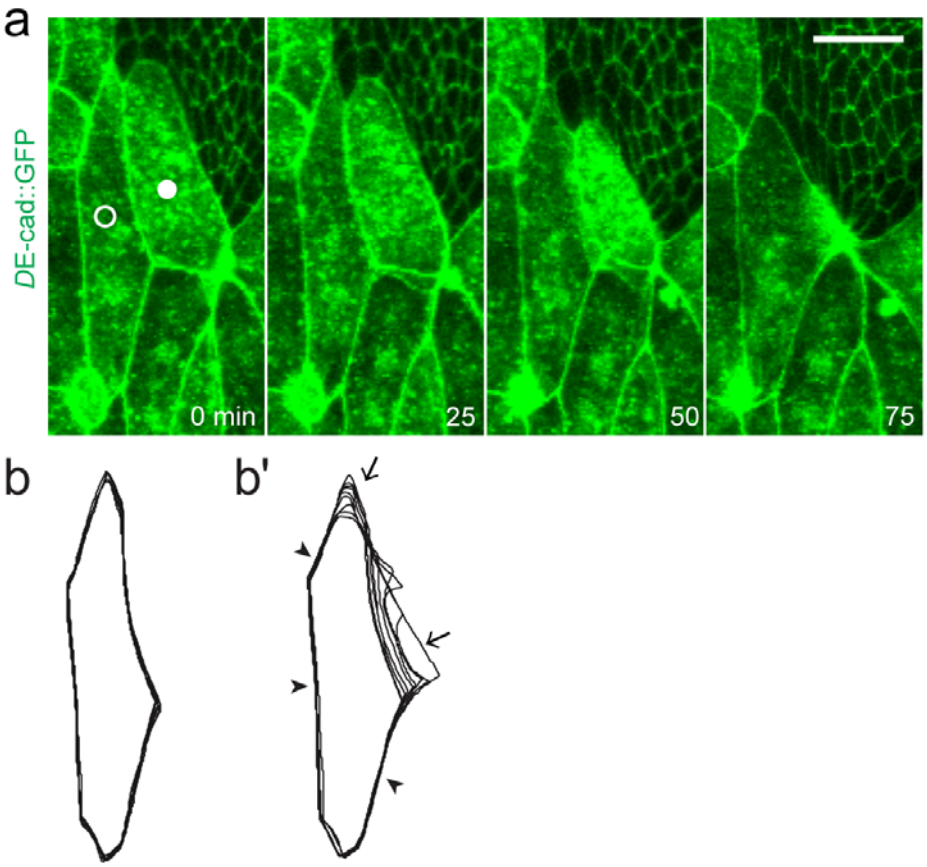

Fig. S5. Kinematics of a LEC next to an apoptotic LEC. Confocal fluorescence images of wild type pupa expressing *D*E-cad::GFP, showing the cell shape deformation of a non-dying LEC (highlighted by open circle), which is next to an apoptotic cell (highlighted by filled circle) and same cell as shown in Fig. 1b. Time stamps denote the same time as shown in Fig. 1b. Scale bar, 20 μm. (b) Contour plots showing the cell shape deformation of the non-dying LEC highlighted in (a) prior to τ_{area} of the apoptotic cell, showing a little deformation. (b') Contour plots of the non-apoptotic LEC from τ_{area} onwards. The cell deformation is local. Arrow indicates the region with major deformation. Arrowheads highlight the cell boundary with little or no deformation.

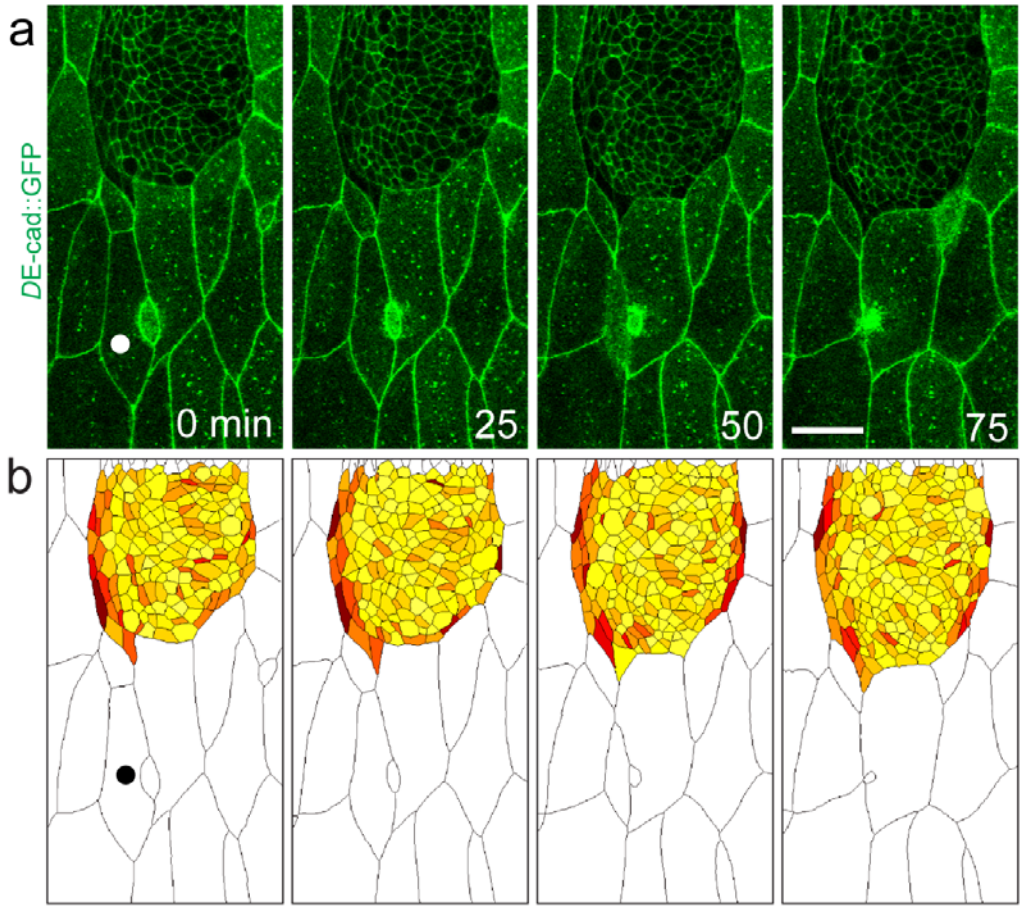

Fig. S6. Mechanical impact of non-boundary LEC apoptosis. (a) Confocal fluorescence images of wild type pupa expressing *D*E-cad::GFP. Non-boundary LEC (i.e., one LEC away from histoblast) is highlighted by filled circles. Scale bars, 50 μm. (b) Color-enhanced reproduction of the confocal images from (a). Colors demote the anisotropy of the cell shape: The darker color represent more elongated histoblast cells (same as Fig. 1c). The color of the histoblasts did not change as much as the case of boundary LEC. Scale bar, 20 μm.

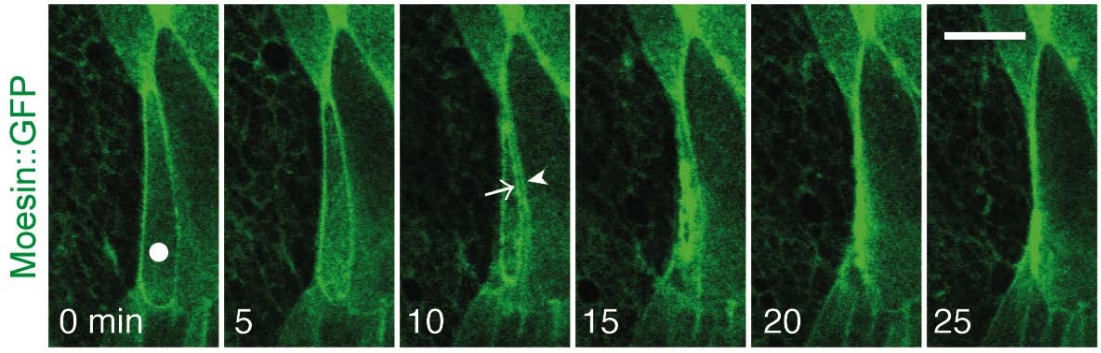

Fig. S7. Actin distribution around the periphery of apoptotic LEC shows two actin cable-like structures. Confocal fluorescence images of wild type pupa expressing Moesin::GFP. Apoptotic LECs are highlighted by filled circles. Arrow and arrowhead show the actin accumulation in the apoptotic LEC and the neighboring non-apoptotic LECs, respectively. Scale bar, 20 μm.

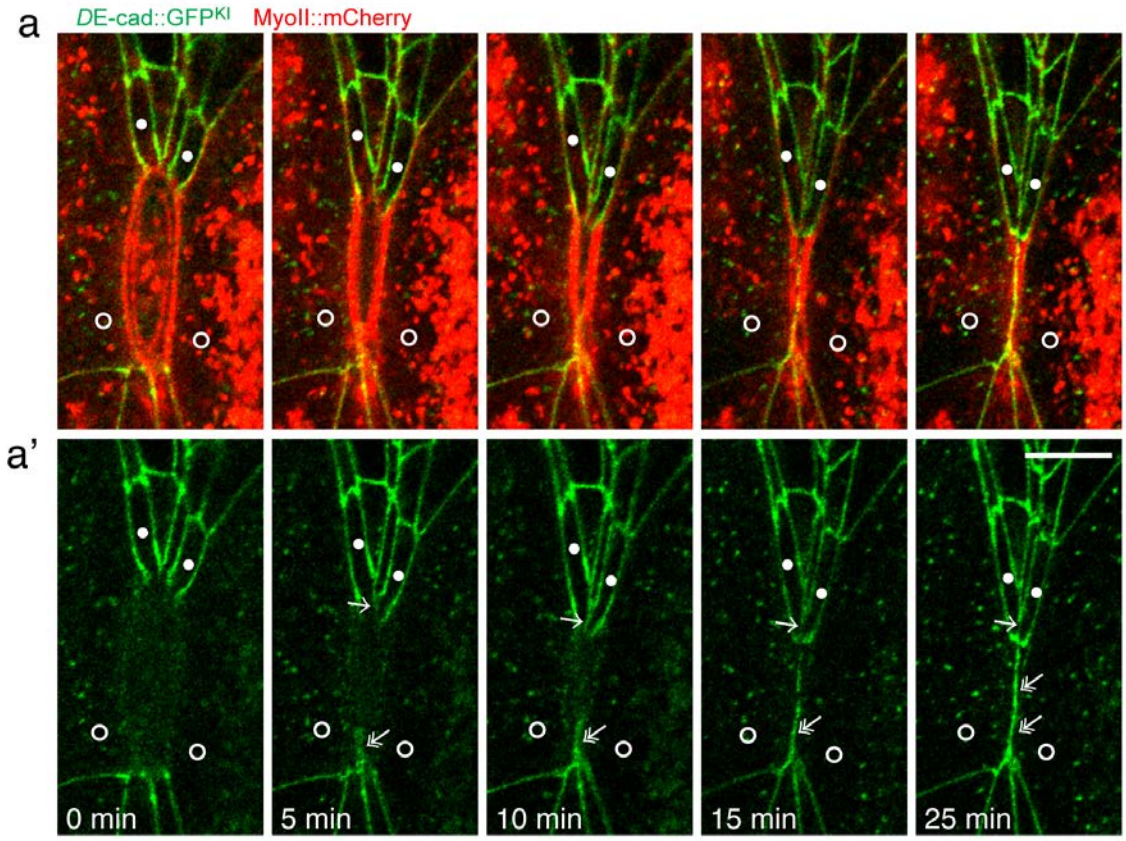

Fig. S8. Formation of *de novo* AJs between the non-apoptotic neighboring cells. Confocal fluorescence images of wild type pupae expressing *D*E-cad::GFP and MyoII::mCherry. Two pairs of neighboring cells (filled and open circles) form *de novo* AJs before the completion of apoptotic cell extrusion (arrows and doublearrows). Scale bar, 10 μm.

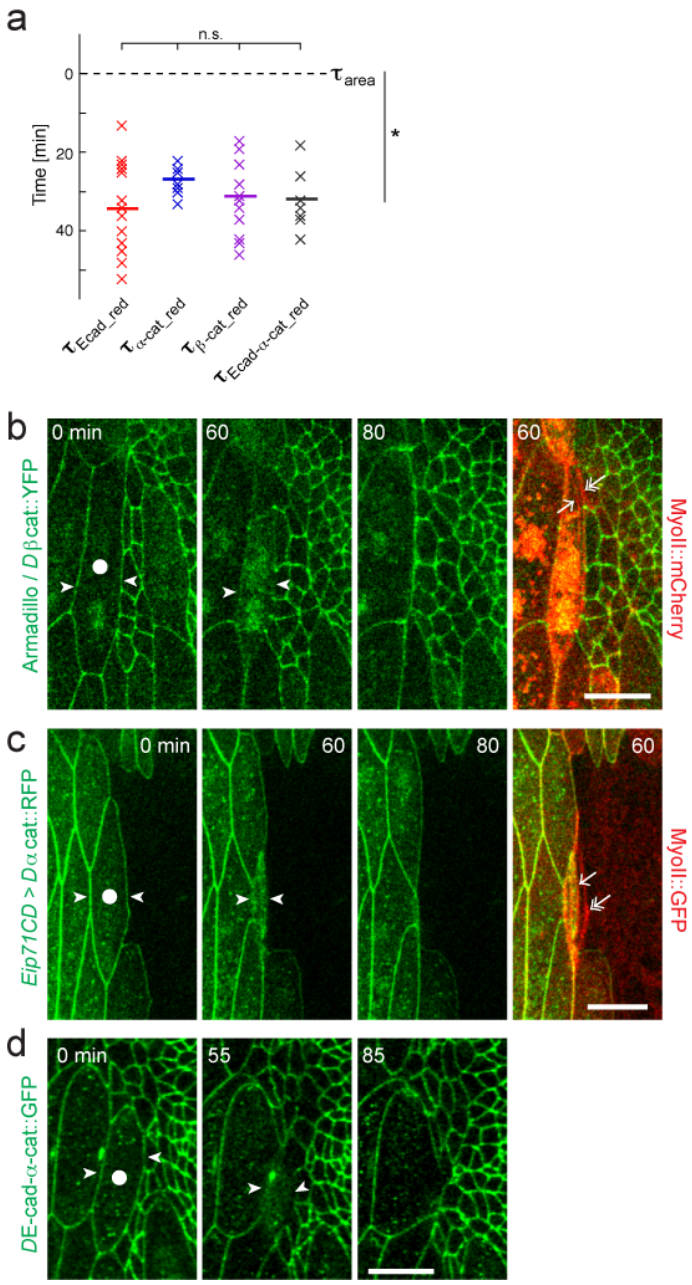

Fig. S9. Reduction of the level of AJ components during apoptosis. (a) Time delays of the reduction of AJ components (τ_{Ecad_red}, $\tau_{\alpha\text{-}cat\_red}$, $\tau_{\beta\text{-}cat\_red}$, and $\tau_{Ecad\text{-}\alpha\text{-}cat\_red}$) using area transition τ_{area} as a reference (*: $P < 0.05$, n.s.: Not significant). n=13, 9, 12, and 7 for τ_{Ecad_red}, $\tau_{\alpha\text{-}cat\_red}$, $\tau_{\beta\text{-}cat\_red}$, and $\tau_{Ecad\text{-}\alpha\text{-}cat\_red}$, respectively. Average values are shown as thick horizontal lines. (b and c) Confocal fluorescence images of wild type pupa expressing *D*β-cat::YFP and MyoII::mCherry (b, Movie 7) or pupa expressing α-cat::RFP only in LECs and MyoII::GFP ubiquitously (c, Movie 8). (d) Confocal fluorescence images of pupa expressing GFP tagged fusion protein that the C-terminal domain of E-cad was replaced by an α-cat protein lacking the N-terminal domain (*D*E-cad-α-cat::GFP). Apoptotic LECs are highlighted by filled circles. Arrowheads shows the dissociation of fluorescence signal. Arrows and double arrows denote the myosin in the apoptotic LEC and the neighboring cells, respectively. Scale bars, 20 μm.

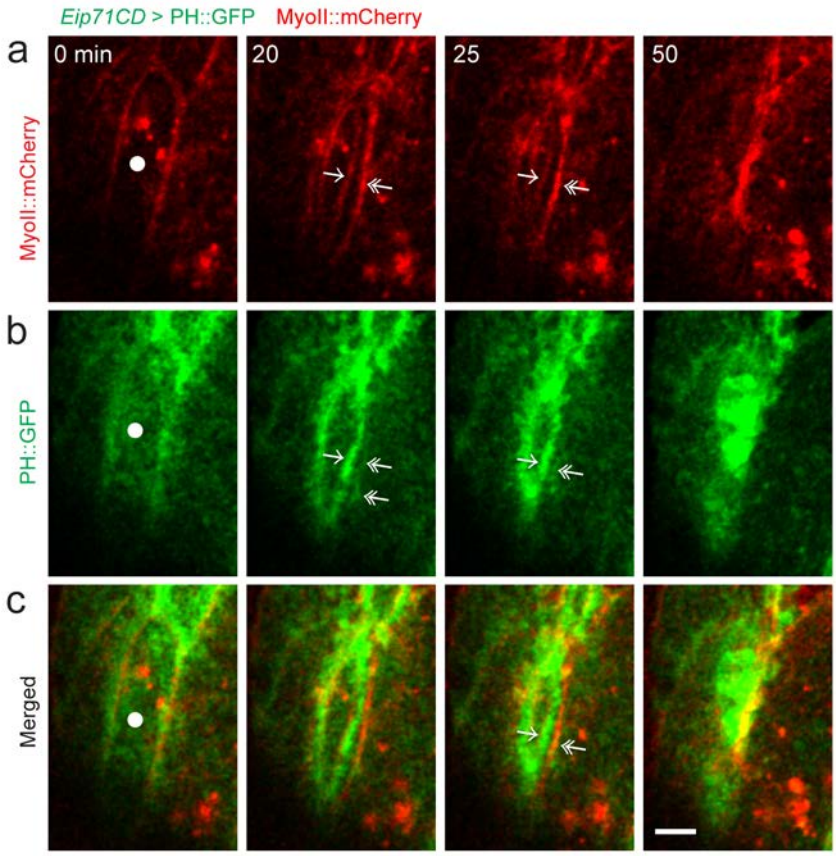

Fig. S10. AJ disengagement upon apoptosis. Confocal fluorescence images of wild type pupa expressing the plasma membrane markers PH::GFP in LECs, and MyoII::mCherry ubiquitously, highlighting the plasma membranes of apoptotic (arrow) and neighboring (double arrows) cells detach once the separation of the two myosin cables become apparent. Same data as shown in Fig. 3g. Scale bar, 20 μm.

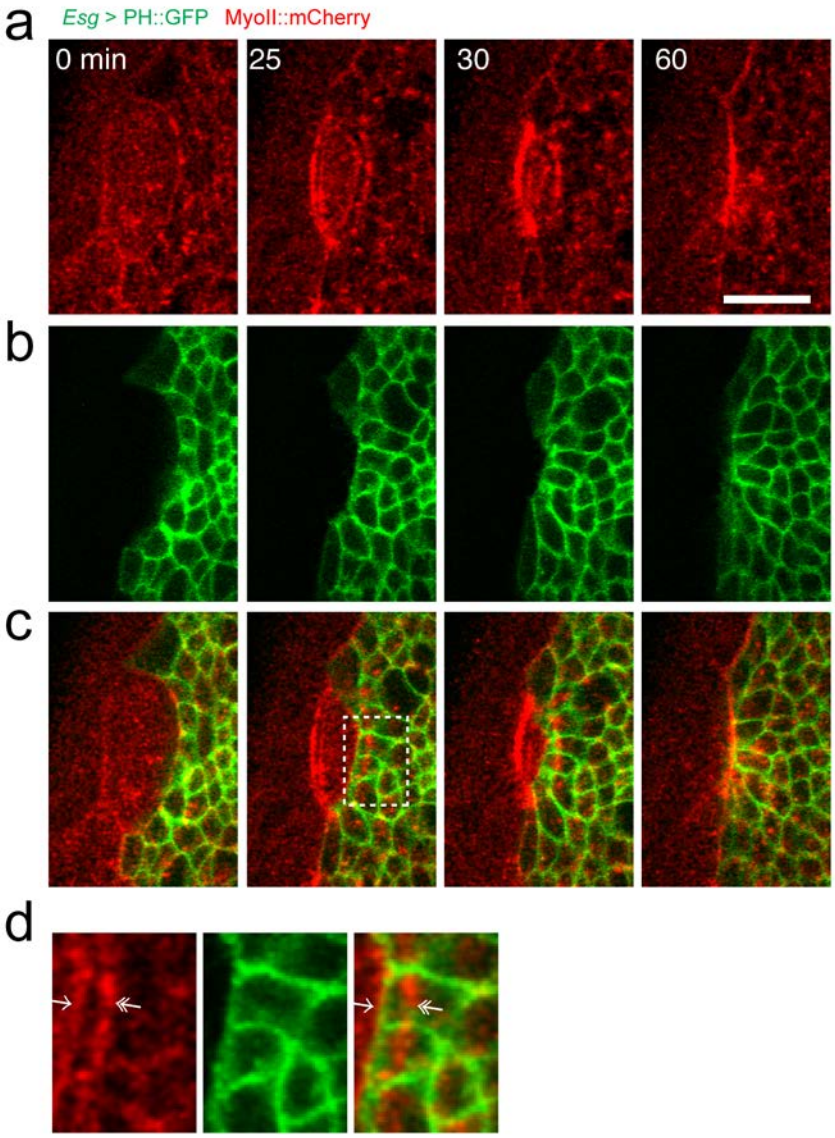

Fig. S11. AJ non-disengagement upon apoptosis. (a-c) Confocal fluorescence images of wild type pupa expressing the plasma membrane markers PH::GFP only in the histoblasts, and MyoII::mCherry ubiquitously. (d) High magnification of the dotted region depicted in (c), highlighting the myosin cable in the apoptotic cell (arrow) and the edge of the histoblast membrane are closely juxtaposed each other. Moreover, the myosin cable in the neighboring cells (double arrowheads) is away from the membrane. Scale bar, 20 μm.

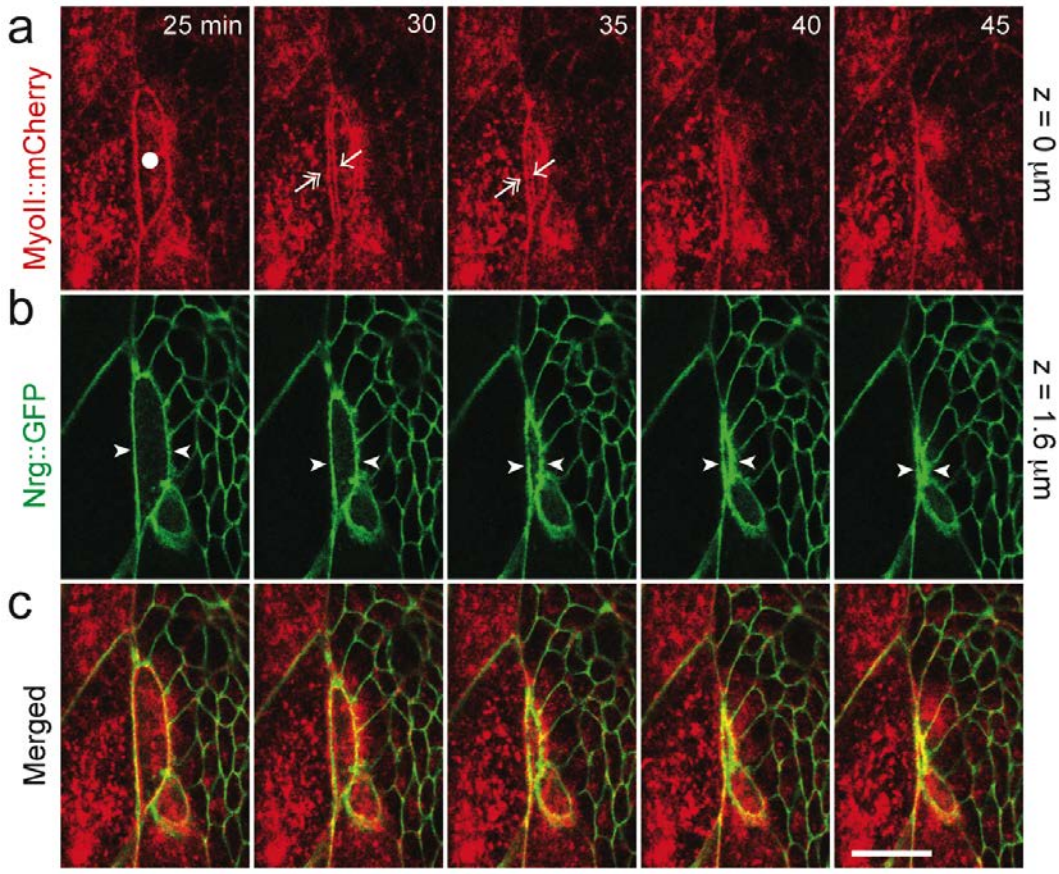

Fig. S12. Dynamics of septate junction (SJ) during LEC apoptosis.
(a-c) Confocal fluorescence images of wild type pupa expressing the septate junction marker Nrg::GFP and MyoII::Cherry (Movie 9). Imaging started at 0 min. (a) MyoII images from a z-section at AJ. Apoptotic LEC is highlighted by filled circles. Arrows and double arrows show the MyoII accumulation in the apoptotic LEC and the neighboring LECs, respectively. (b) Images of the septate junction from a z-section 1.6 μm below AJ. Arrowheads indicate the septate junction is not compromised during the apical constriction of the apoptotic cell. (c) Merged image. Scale bar, 20 μm.

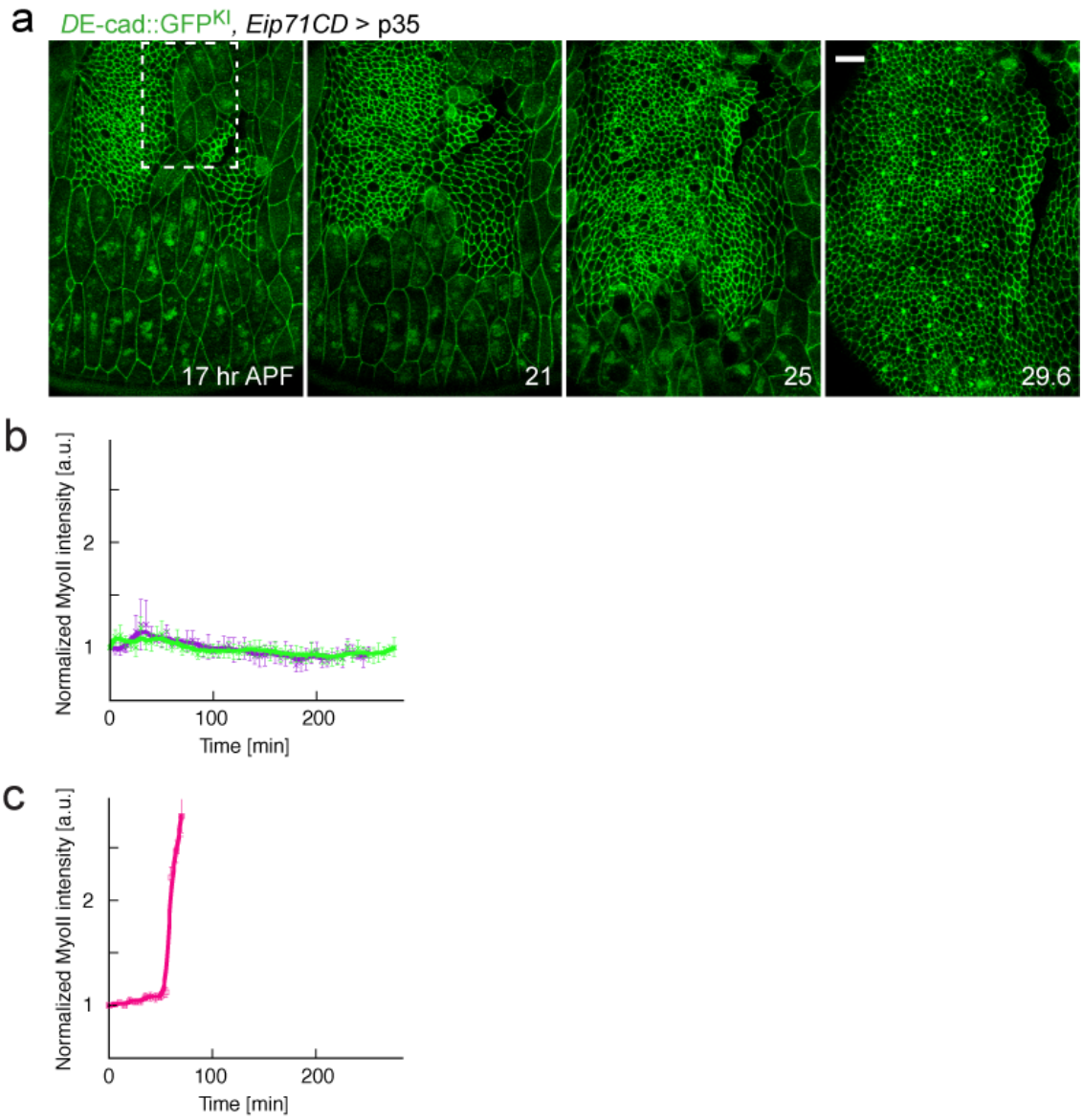

Fig. S13. Extrusion of LECs expressing caspase inhibitor. (a) Confocal fluorescence images of pupa expressing caspase inhibitor p35 only in LECs, and *D*E-cad::GFP^{KI} ubiquitously, showing anterior and posterior dorsal histoblast nests and LECs at 17, 21, 25, and 29.6 hours APF. White dotted region represent the field shown in Fig. 5a. Scale bars, 20 μm. (b) Graphs plotting normalized MyoII intensity of extruding cell (green, n=5) and of the summation of extruding cell and neighboring cell (purple, n=7) over time. (c) Graphs plotting normalized MyoII intensity of the summation of apoptotic cell and neighboring cell in wild-type pupae (pink, n=6) over time. Error bars indicate SEM.

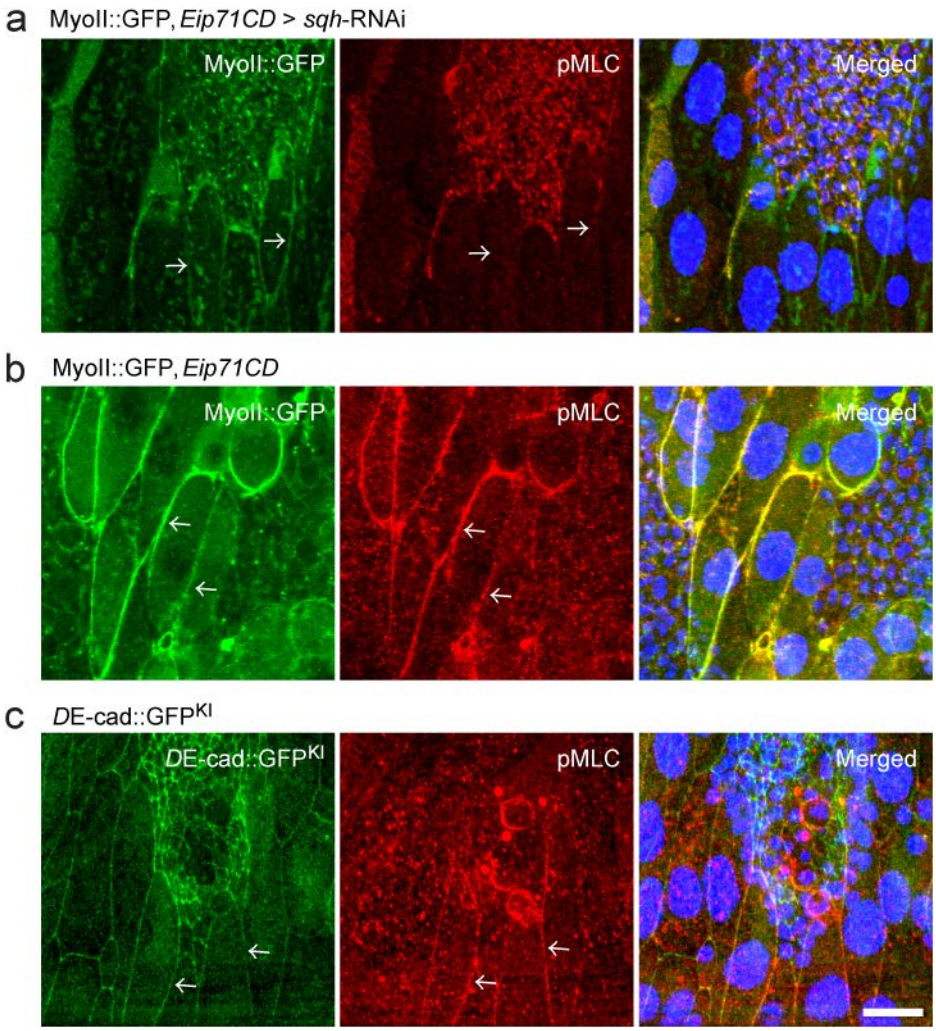

Fig. S14. Level of phosphorylated myosin regulatory light chain in different pupae. (a-c) Confocal fluorescence images of pupae stained with phosphorylated myosin regulatory light chain (pMLC, red) and DAPI (blue). (a) Images of pupa expressing sqh-RNAi only in LECs, and MyoII::GFP ubiquitously. (b and c) Images of control pupa expressing MyoII::GFP (b) and *D*E-cad::GFP^{KI} (c), ubiquitously. The level of pMLC at cell boundaries (arrows) in sqh-RNAi expressing LECs is weaker than that of control LECs. Scale bar, 20 µm.

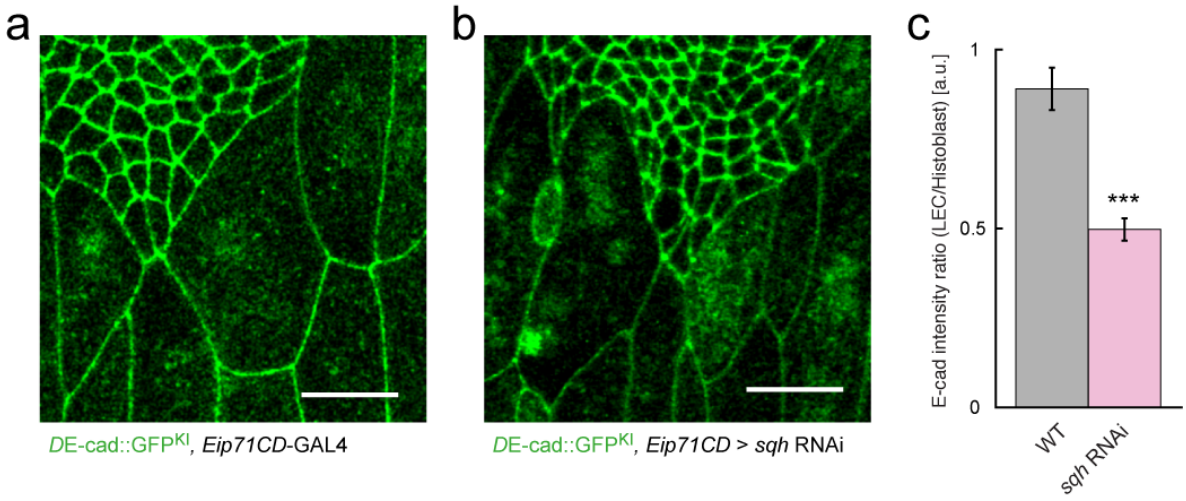

Fig. S15. Level of E-cad in LECs expressing *sqh*-RNAi.
(a, b) Confocal fluorescence images of wild-type pupa expressing *D*E-cad::GFP^{KI} ubiquitously (a) or pupa expressing *sqh*-RNAi only in LECs and *D*E-cad::GFP^{KI} ubiquitously (b). The contrast of the images were adjusted so that the fluorescence intensity of histoblasts became equivalent. No apoptotic cells are shown in both images. (c) Statistical comparison of the ratio of E-cad intensity between LEC and histoblast. Gray and light red bars denote the mean values from wild-type and sqh-RNAi expressing LECs, respectively (n=5 and 8). Each ratio was calculated based on the average of 20 cell boundaries of LECs and histoblast from an image. Scale bars, 20 μm

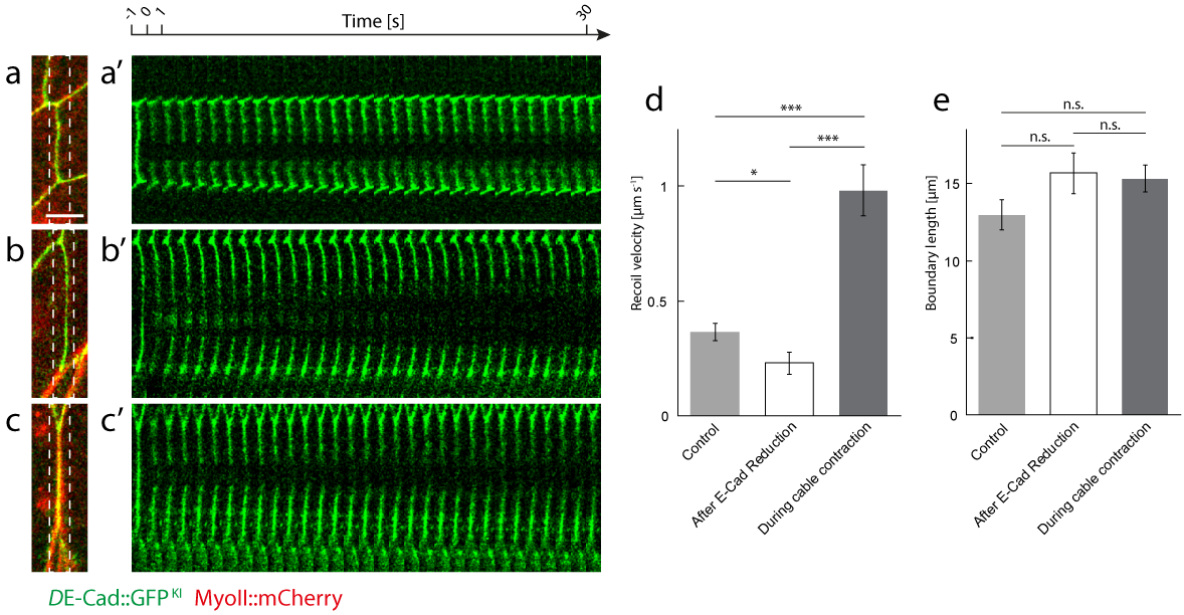

Fig. S16. Tissue tension release and reshape after reduction of E-cad levels in LECs. (a-c) Confocal fluorescence images of wild-type pupa expressing *D*E-cad::GFP^{KI} and MyoII::mCherry ubiquitously highlighting the LEC boundaries connected to the apoptotic LEC before ablation. (a'-c') Kymographs generated from the white boxed regions in a-c, showing the dynamics of the cell boundaries after ablation. The ablations were performed in three different stages of apoptotic cell extrusion: before reduction of E-cad levels (a and a'); right after reduction (b and b'); and during neighboring actomyosin cable (double-arrow in c) contraction (c and c'). Scale bar, 10 μm. Statistical comparison of the recoil velocities (d) and the length of cell boundary at laser ablation (e) at each stage of cell extrusion shown in a-c. n=16, 11 and 13 for control, after reduction, and, during cable contraction, respectively. Error bars indicate SEM. *: $P < 0.05$, ***: $P < 0.001$, n.s.: no significance.

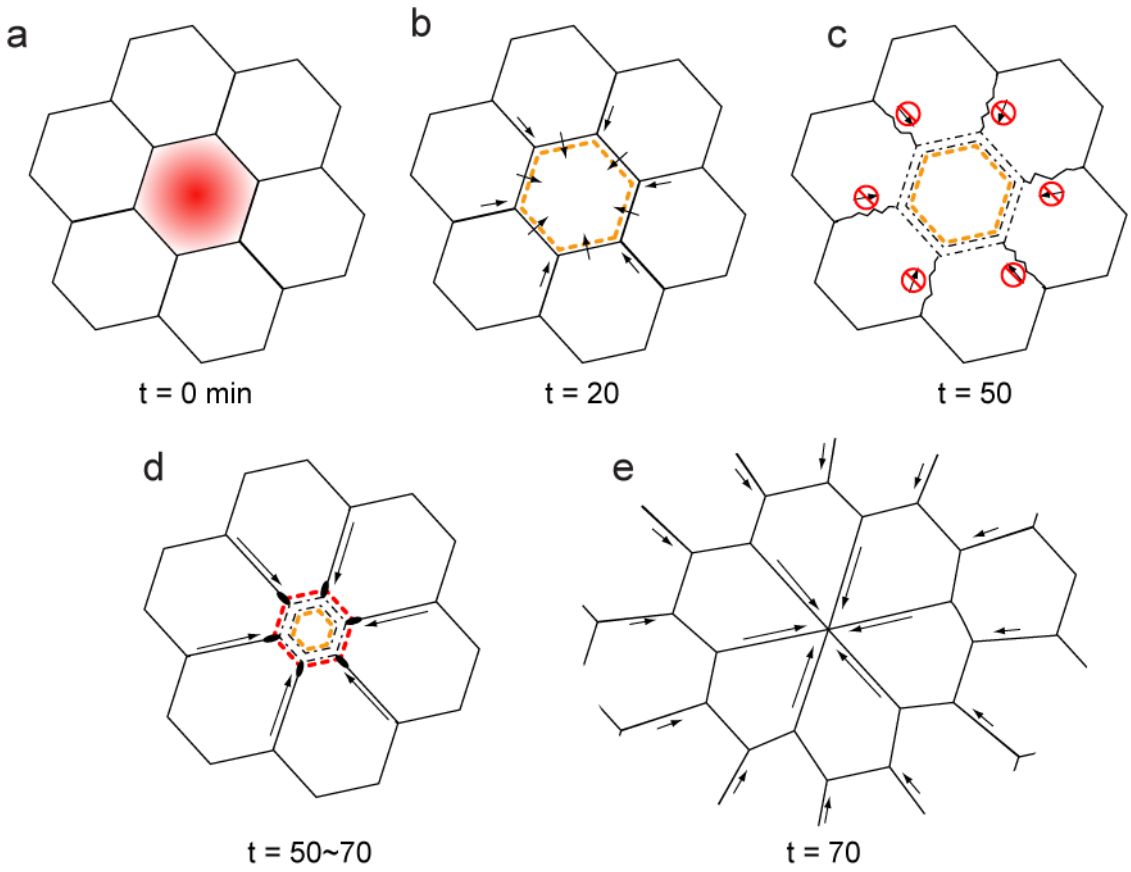

Fig. S17. A model of the progressive remodeling of AJ and tissue tension during apoptosis. Cartoons show the progression of apoptotic events with the top view at the AJ. Cell size and shape are not scale. (a) Caspase activation (set this time as t=0min). (b) Beginning of apical constriction and MyoII accumulation (orange dotted line) in the apoptotic cell (t=20min). The contraction of the actomyosin cable pulls the neighboring cells through the AJ (black arrows). (c) AJ disengagement (black dotted lines) and tension release (t=50min). (d) MyoII accumulation in neighboring non-apoptotic cells (red dotted lines). Contraction of supra-cellular actomyosin cables reshape the tissue tension (black arrows) (t=50-70min). (e) End of apical constriction. The propagation of mechanical force promotes tissue dynamics (black arrows) (t=70min).

Supplementary Materials and Methods

Drosophila stocks and Genetics

Otherwise stated, fly stocks were obtained from the Bloomington Stock Center. The following lines were used: *ubi*-E-cad::GFP (H. Oda), Nrg::GFP (Kyoto Stock Center), moe::GFP (D. Kiehart), *ubi*-E-cad::GFP; *sqh*-*Sqh*-mCherry (A.C. Martin), Armadillo::YFP , and Knock-in alleles of *D*E-cad::GFP and *D*E-cad::mTomato (Huang et al., 2009). The following UAS and GAL4 were used to ectopically express the gene of interest: UAS-*sqh*::GFP (M. Affolter), UAS-α-catenin::RFP (K. Sugimura), UAS-*sqh*-RNAi (VDRC), UAS-SCAT3 (M. Miura), UAS-p35, *Esg*-GAL4, *Eip71CD*-GAL4, and *tsh*-GAL4. Live imaging of E-cad and caspase-3 sensor SCAT3 was carried out by crossing *tsh*-GAL4, UAS-SCAT3/CyO (M. Miura) with *D*E-cad::mTomato (Huang et al., 2009).
sqh-RNAi MARCM clones that were positively marked by the double copy of histone-RFP expression were recovered from neoFRT19A, *tubP*-Gal80, *hs*FLP; UAS-*sqh*-RNAi (male), and neoFRT19A, *ubi*-mRFP.nls; *ubi*-E-cad::GFP, *Eip71CD*-GAL4 (female). Mitotic clones were induced using the FLP-FRT technique by using the *hs*-FLP with heat shock for 50 min at 37°C in early embryos. The genotypes of three cells analyzed in Fig. 7b are, neoFRT19A, tubP-Gal80, hsFLP/neoFRT19A, ubi-mRFP.nls; UAS-sqh-RNAi/ DE-cad::GFP-KI, Eip71CD-GAL4; +/+ ($LEC_{WT/WT}$), neoFRT19A, tubP-Gal80, hsFLP/neoFRT19A, tubP-Gal80, hsFLP; UAS-sqh-RNAi/ DE-cad::GFP-KI, Eip71CD-GAL4; +/+ ($LEC_{WT/RNAi}$), and neoFRT19A, ubi-mRFP.nls/neoFRT19A, ubi-mRFP.nls; UAS-sqh-RNAi/ DE-cad::GFP-KI, Eip71CD-GAL4; +/+ (LEC_{RNAi}).

Cell shape anisotropy analysis

To measure the anisotropy of individual histoblast cell (Fig. 1c and Fig. S1), the z-projected E-cad::GFP time-lapse images were first segmented by Packing Analyzer V2.0 (Aigouy et al., 2010). The cell boundary data were subsequently analyzed with Matlab software (MathWorks, MA, USA). Segmented cell shapes were fitted by ellipse, which was optimized by maximizing the area overlap between a segmented cell shape and an ellipse. Anisotropy of the cell was defined as the ratio of minor and major axes of the fitting ellipse.

Caspase-3 activity analysis

To monitor caspase-3 activity (Fig. 2a and Movie 5), fly with FRET base caspase-3 sensor, SCAT3 (Nakajima et al., 2011, Takemoto et al., 2003) was used. A 405nm laser was used to excite ECFP and two fluorescence images (ECFP and Venus) were simultaneously captured. FRET ratio was calculated by taking the intensity ratio between the sum-intensity z-projected ECFP and Venus images. FRET ratio of an apoptotic LEC (Fig. 2c) was measured by averaging the FRET ratio within an apoptotic cell. The shape of an apoptotic cell was manually segmented from the sum-intensity z-projected Venus images over time by using ImageJ (Schneider et al., 2012).

Determination of the transition time

To measure the time delay between the beginning of apical constriction and caspase-3 activation (Fig. 2c), we first normalized the cell area and caspase-3 activity data to the value measured at time = 0 sec (Fig. S3a). The area data was shifted in time to minimize the difference between area and caspase-3 data (Fig. S3b). The shift was defined as Δt_{shift}.

To determine when the cell started to constrict with higher speed (τ_{area}) and when the cell started to activate its Cas-3 activity (τ_{Cas3}) without comparing the two graphs, we referred to the maximum derivative of each graphs. We defined τ_{area} as the time when the derivative of the graph reached to 25% of the maximum slope (Fig. S3c). Similarly, we defined τ_{Cas3}. The time delay between the initiation of apical constriction and caspase-3 activation measured by 25% of maximum slope, $\Delta t_{25\%} = |\tau_{area} - \tau_{Cas3}|$, was consistent to Δt_{shift} (Fig. S3d). With the other values, e.g., numbers between 10% and 40%, $|\tau_{area} - \tau_{Cas3}|$ was not as close to Δt_{shift} as 25%.

Same setting (25% of the maximum slope) was used to define the transition time not only for τ_{area} and τ_{Cas3}, but also for all the other data, for instance τ_{EcadKI}, τ_{outer_MyoII} and τ_{inner_MyoII}.

MyoII intensity analysis

To quantify the progression of MyoII accumulation in apoptotic LECs or neighboring cells, the average fluorescent intensity of MyoII::GFP signal either from histoblast that originally attached to apoptotic LEC (Fig. 4a') or solely originated from the cell periphery of apoptotic LECs (Fig. 4c') were measured. Images of sum-intensity z-projection (around AJ) of MyoII::GFP were analyzed over time. ROIs (see main text for more detail) to calculate the intensity were manually defined by the free-hand line tools of ImageJ. The total intensity along the line with thickness of 4 pixels (0.24 μm/pixel) was measured and divided by the length of the line.

Cell boundary linearity measurement

Linearity of the histoblast cell boundaries was calculated as a ratio of the two ends of boundary (measured by using ImageJ Straight Line tool) to the actual length of the histoblast cell boundary (measured by using ImageJ Segmented Line tool). A linearity value 1 represents a straight line.

Calculation of initial recoil velocity after ablation

The length of ablated cell boundary was measured overtime by using ImageJ Straight Line tool. Data points before the cut were fit with linear line. An exponential was used to fit the data after the cut. The effective time of the cut was found as the intersection of the linear line with the exponential. The initial recoil velocity was found from the deliberative of the exponential at effective time of the cut. The velocity was calculated in Matlab. More detail can be found in (Hara et al., 2016).

Quantitative analyses of the deformation in the shape of extruding LECs

To quantify the local/isotropic deformation of extruding LEC, as shown in Fig. 1e (before τ_{area}) and 1e' (after τ_{area}), we first measured the differences in cell shapes at two different time points (Fig. S4a). Before τ_{area}, the differences in cell shapes at [τ_{area}-25] min and τ_{area} min was shown as gray area in Fig. S4a (left). The centoid of this gray area (residual area) and the cell area at τ_{area} (white area) were shown as a red and black cross, respectively. We then defined the black cross as the origin of the new coordinate system. We further rotated the coordinate so that y-axis represented the direction toward histoblast. After τ_{area}, the differences in cell shapes at τ_{area} min and [τ_{area}+25] min was shown as gray area in Fig. S4a (right). The centoid of this gray area (residual area) and the cell area at [τ_{area}+25] (white area) were shown as a blue and black cross, respectively. Finally, we analyzed 6 cells before and after τ_{area}, and summarized all data in a same graph (Fig. S4b).

Supplemental References

Aigouy, B., Farhadifar, R., Staple, D.B., Sagner, A., Roper, J.C., Julicher, F. & Eaton, S. (2010). Cell flow reorients the axis of planar polarity in the wing epithelium of Drosophila. *Cell,* 142**,** 773-86.

Hara, Y., Shagirov, M. & Toyama, Y. (2016). Cell Boundary Elongation by Non-autonomous Contractility in Cell Oscillation. *Current biology : CB,* 26**,** 2388-96.

Huang, J., Zhou, W., Dong, W., Watson, A.M. & Hong, Y. (2009). Directed, efficient, and versatile modifications of the Drosophila genome by genomic engineering. *Proceedings of the National Academy of Sciences,* 106**,** 8284-8289.

Nakajima, Y.-I., Kuranaga, E., Sugimura, K., Miyawaki, A. & Miura, M. (2011). Nonautonomous Apoptosis Is Triggered by Local Cell Cycle Progression during Epithelial Replacement in Drosophila. *Molecular and Cellular Biology,* 31**,** 2499-2512.

Schneider, C.A., Rasband, W.S. & Eliceiri, K.W. (2012). NIH Image to ImageJ: 25 years of image analysis. *Nature methods,* 9**,** 671-5.

Takemoto, K., Nagai, T., Miyawaki, A. & Miura, M. (2003). Spatio-temporal activation of caspase revealed by indicator that is insensitive to environmental effects. *The Journal of cell biology,* 160**,** 235-43.

Supplemental Movies

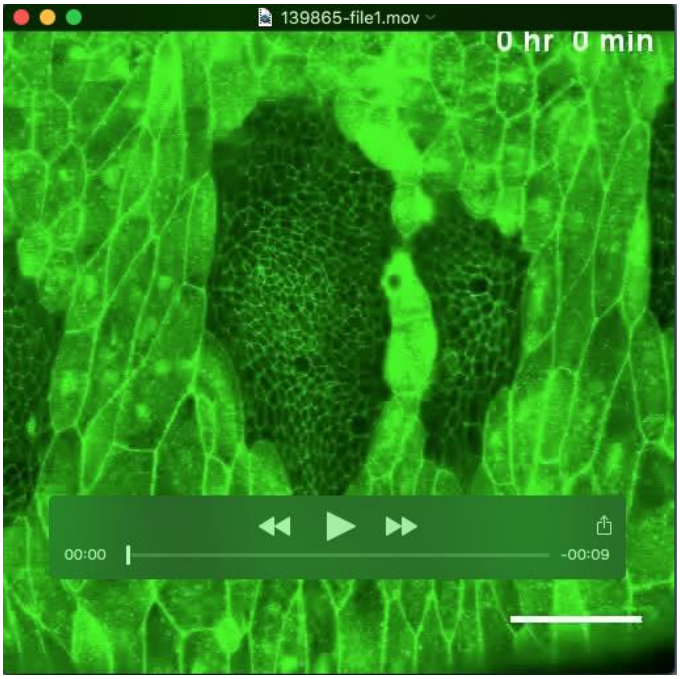

Movie 1. Time-lapse images of wild-type pupa expressing *ubi-D*E-cad::GFP. Scale bar, 50 µm.

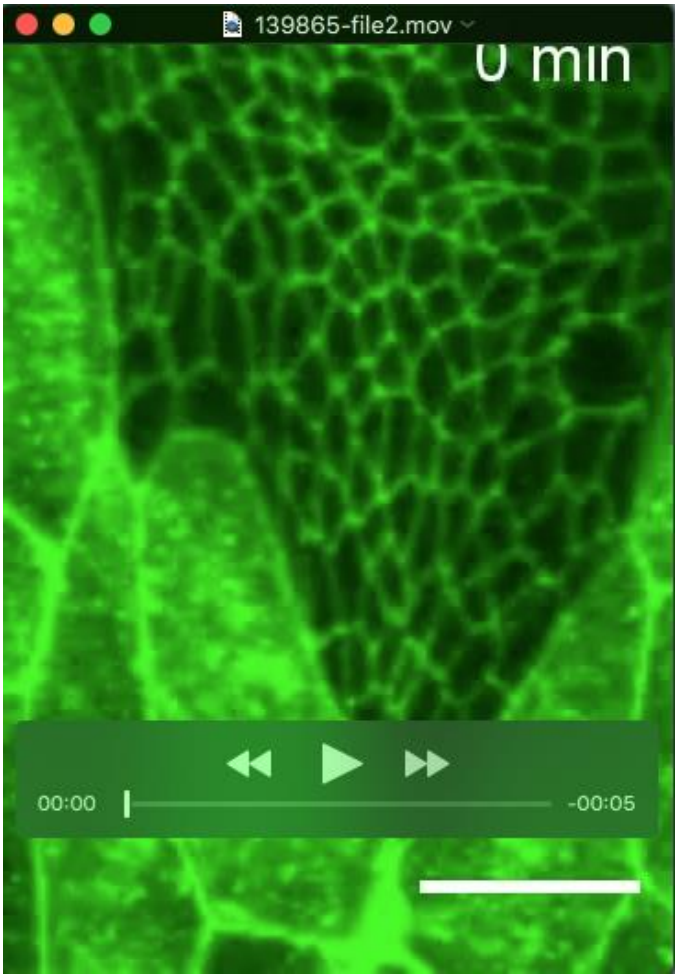

Movie 2. Time-lapse images of wild-type pupa expressing *ubi-D*E-cad::GFP. Scale bar, 20 μm.

Movie 3. Time-lapse images of wild-type pupa expressing Lifeact::GFP. Top view and orthogonal views. Scale bar, 20 µm.

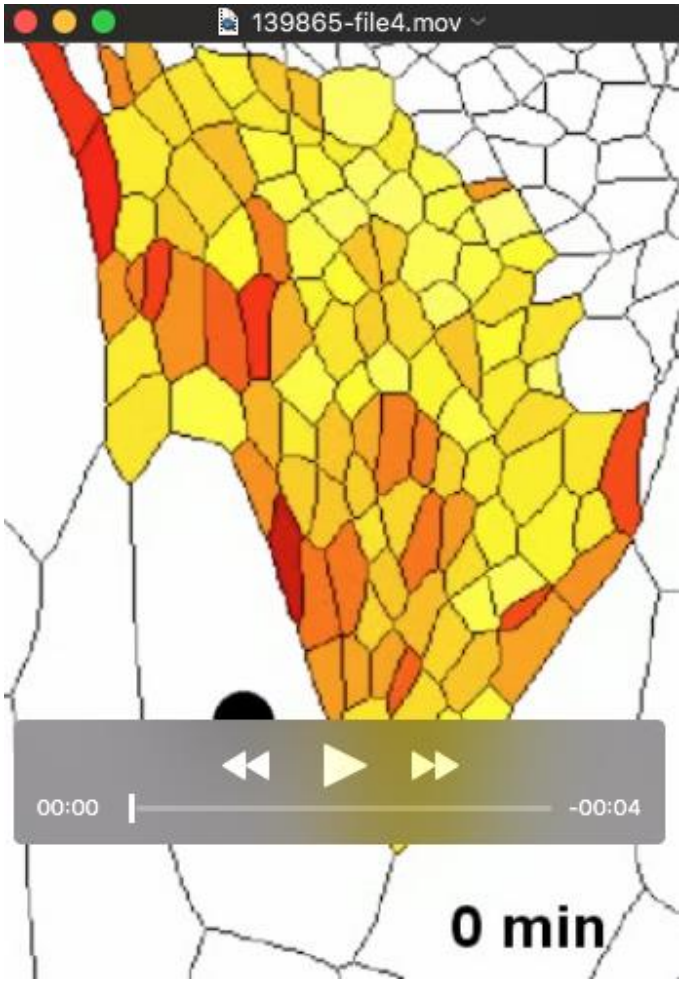

Movie 4. Color-enhanced reproduction of the confocal images from Movie 3. Colors demote the anisotropy of cell shape (as illustrated by the color bar in Fig. 1c).

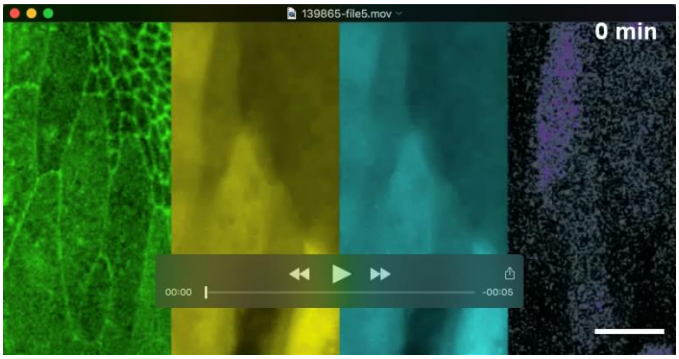

Movie 5. Time-lapse images of wild-type pupa expressing *D*E-cad::mTomato^{KI} (green), FRET-base caspase-3 sensor SCAT3 (Venus: yellow, ECFP: cyan), and FRET ratio (perple - white). Scale bar, 20 μm.

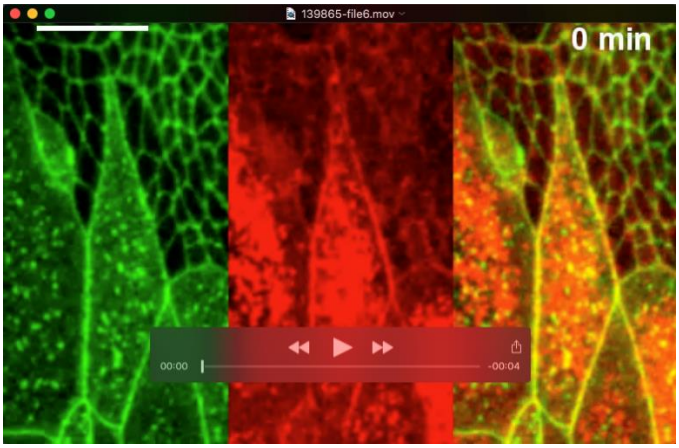

Movie 6. Time-lapse images of of wild-type pupa expressing *ubi-D*E-cad::GFP (green) and MyoII::Cherry (red). Scale bar, 20 μm.

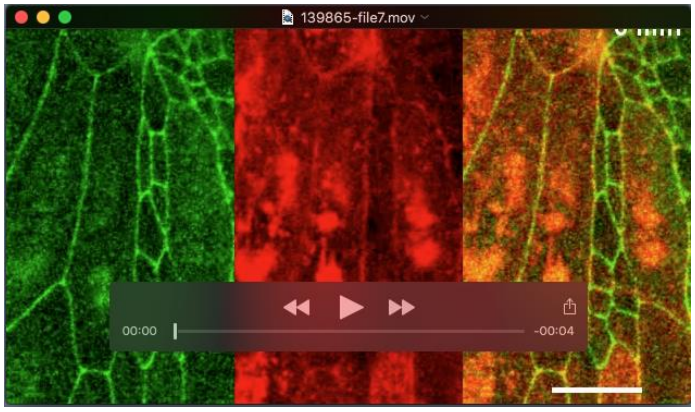

Movie 7. Time-lapse images of wild-type pupa expressing β-cat::YFP (green) and MyoII::Cherry (red). Scale bar, 20 μm.

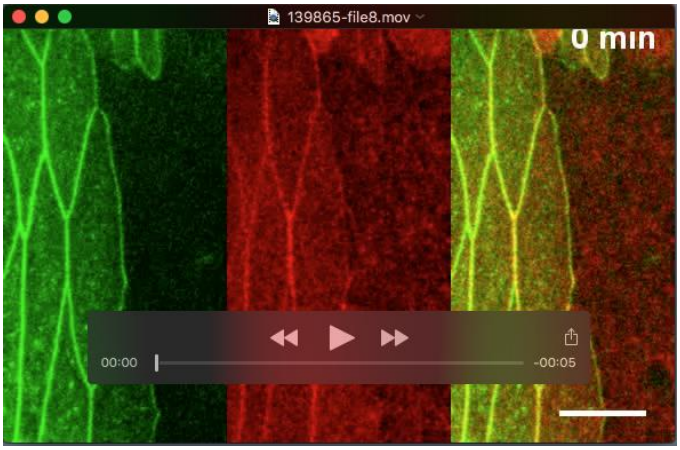

Movie 8. Time-lapse images of wild-type pupa expressing α-cat::RFP (green) and MyoII::GFP (red). Scale bar, 20 μm.

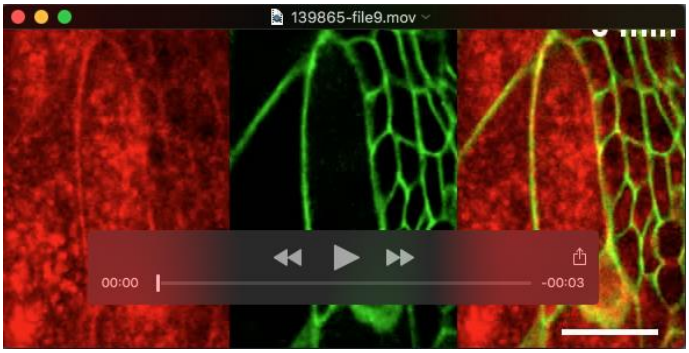

Movie 9. Time-lapse images of wild-type pupa expressing Nrg::GFP (green) and MyoII::Cherry (red). Scale bars, 20 μm.

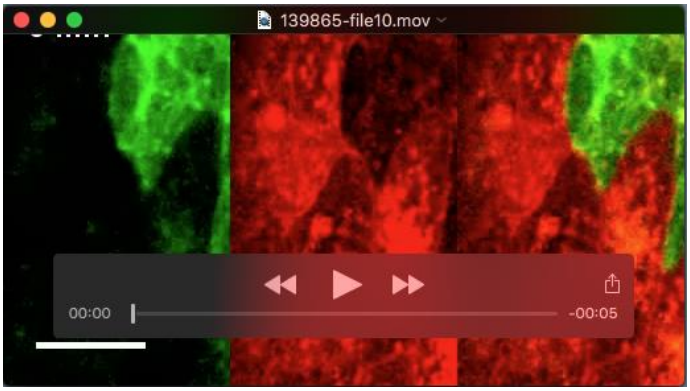

Movie 10. Time-lapse images of wild-type pupa expressing MyoII::GFP in histoblasts (green) and MyoII::Cherry (red) ubiquitously. Scale bar, 20 μm.

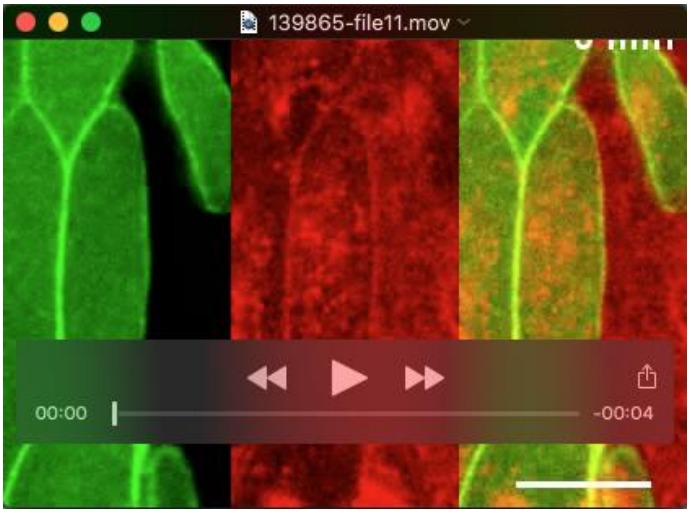

Movie 11. Time-lapse images of wild-type pupa expressing MyoII::GFP in LECs (green) and MyoII::Cherry (red) ubiquitously. Scale bar, 20 µm.

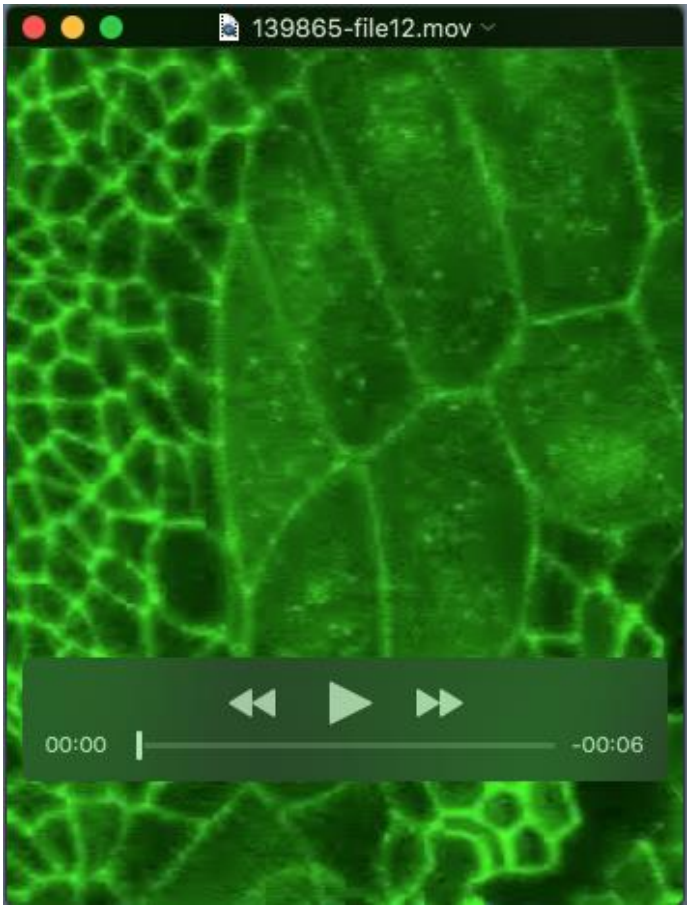

Movie 12. Time-lapse images of pupa expressing caspase inhibitor p35 only in LECs and expressing E-cad::GFP^{KI} (green) ubiquitously. Scale bar, 20 µm.

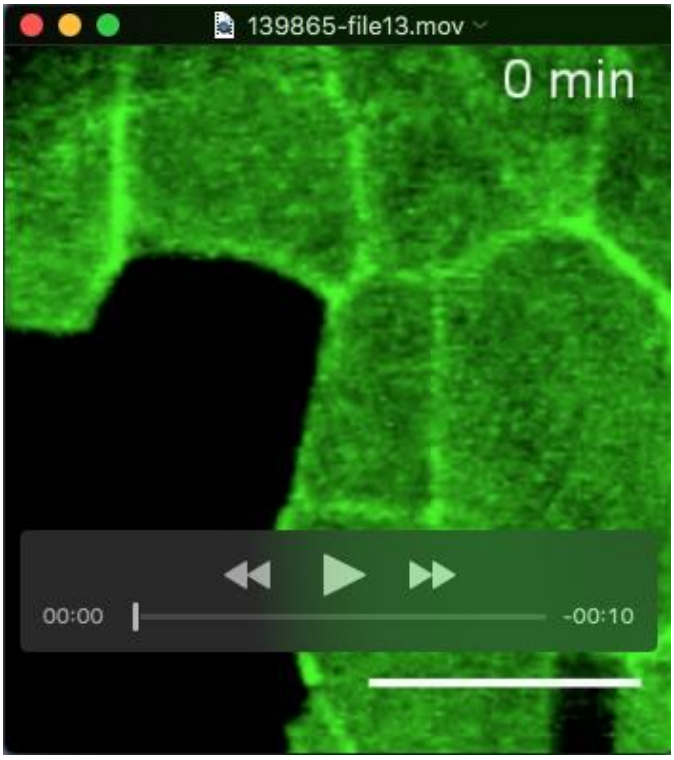

Movie 13. Time-lapse images of pupa expressing caspase inhibitor p35 and MyoII::GFP (green) only in LECs. Scale bar, 20 μm.

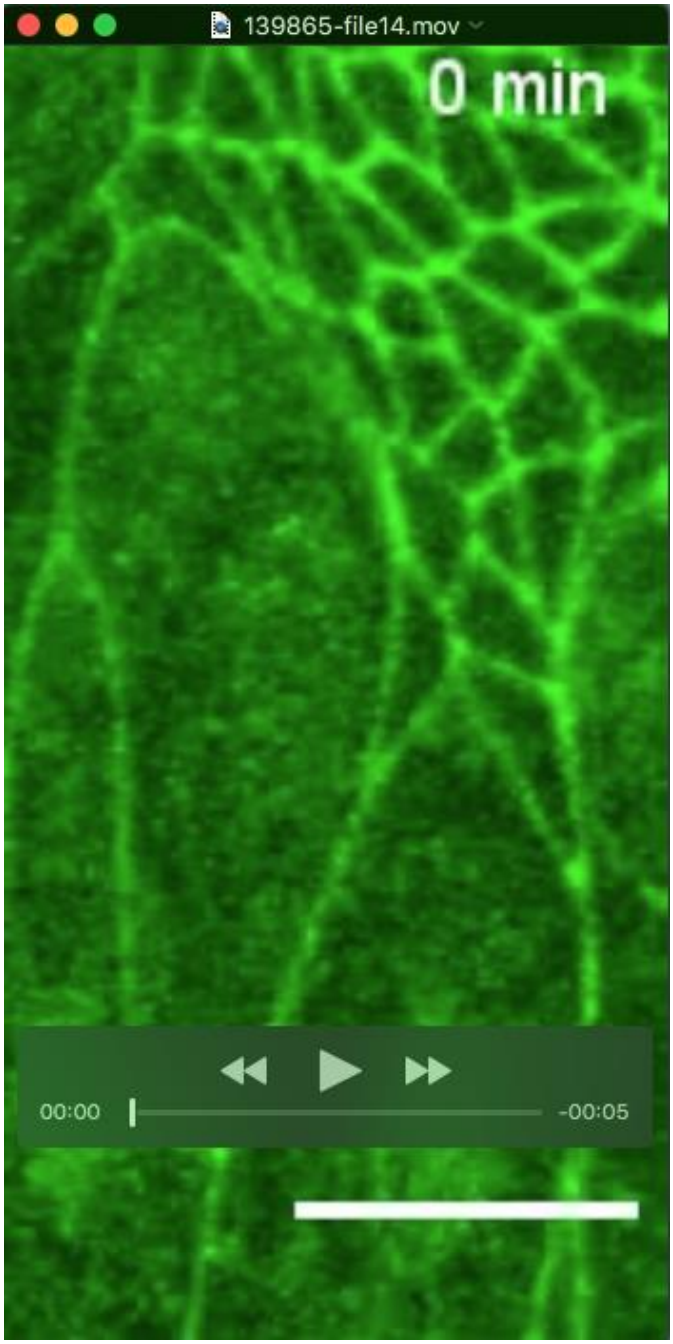

Movie 14. Time-lapse images of pupa expressing sqh-RNAi only in LECs and expressing E-cad::GFP^{KI} (green) ubiquitously. Scale bar, 20 μm.

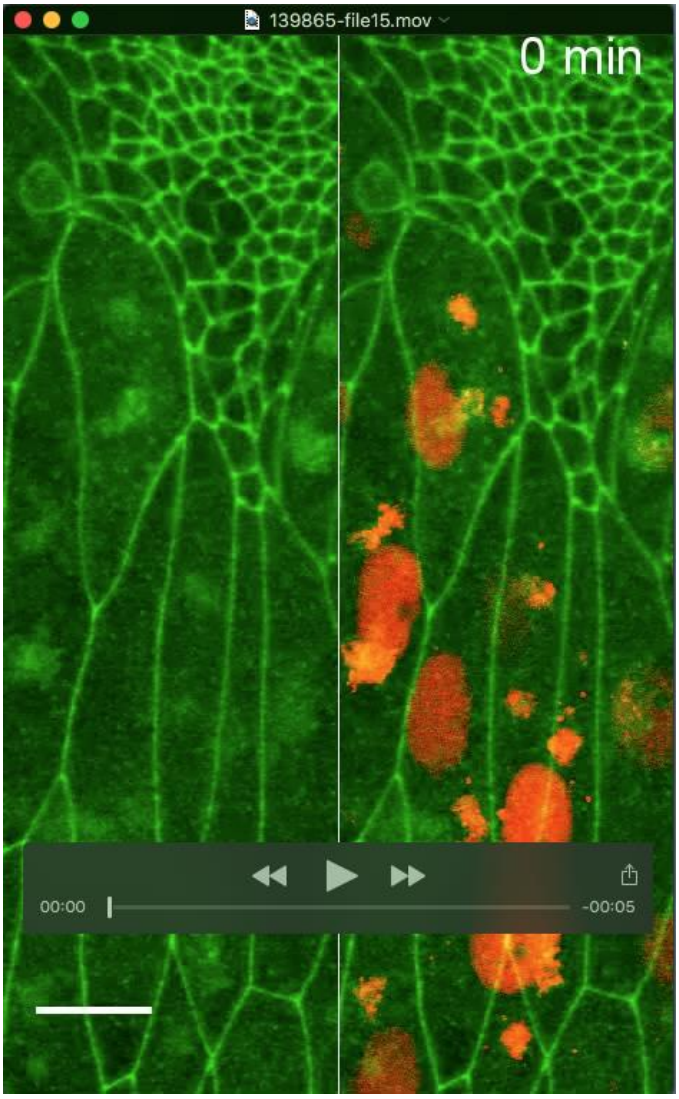

Movie 15. Time-lapse images of pupa with clonal expression of *sqh*-RNAi. E-cadherin::GFP (green) and Histone::Cherry (red). Scale bar, 20 μm.

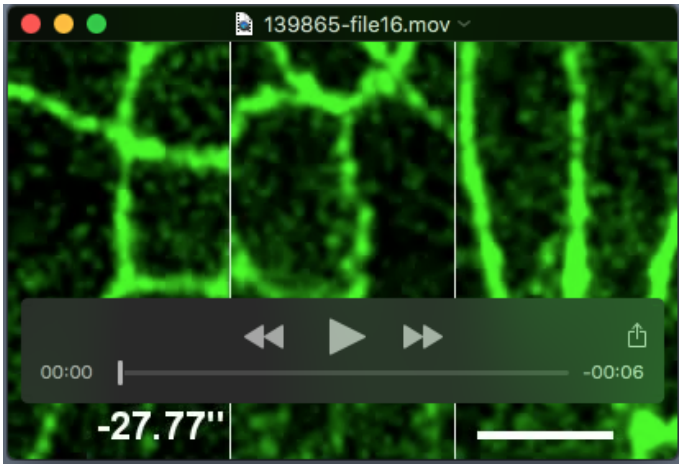

Movie 16. Time-lapse images of laser ablation on pupa with *D*E-cad::GFP. The ablations were performed in three different stage of apoptotic cell extrusion: before the reduction of E-cad (left); right after the reduction of E-cad (middle); and during the contraction of actomyosin cable in the neighboring cells (right). Scale bar, 5 μm.